Astron. Astrophys. 335, 266–276 (1998)

ASTRONOMY AND ASTROPHYSICS

Methanol in protostellar outflows

Single-dish and interferometric maps of NGC 1333/IRAS 2

R. Bachiller[1], **C. Codella**[1], **F. Colomer**[1], **S. Liechti**[1], **and C.M. Walmsley**[2]

[1] Observatorio Astronómico Nacional (IGN), Apartado 1143, E-28800 Alcalá de Henares (Madrid), Spain
[2] Osservatorio Astrofisico di Arcetri, Largo E. Fermi 5, I-50125 Firenze, Italy

Received 18 December 1997 / Accepted 16 March 1998

Abstract. We report high-resolution mapping observations of the 2_k–1_k, 3_k–2_k, and 5_k–4_k thermal lines of CH_3OH toward the young bipolar outflow driven by the Class 0 object NGC 1333/IRAS 2. Only weak emission has been detected towards the position of the central object, while strong methanol lines have been observed towards the endpoints of the outflow lobes, where the CH_3OH abundance is enhanced by a factor ~ 300. The methanol emission is confined in two jets, with a collimation factor of about 20: redshifted emission comes from the south-east lobe, while blueshifted lines are detected towards the north-west. Statistical equilibrium calculations have been used to fit the relative intensities of the observed transitions. These lead us to the conclusion that the ambient gas surrounding the protostar has a density similar to that of the high velocity gas in the shocked regions ($\sim 10^6$ cm^{-3}).

Interferometric maps with a resolution of $3''$ show that the blueshifted lobe consists of several "bullets" indicating that episodic mass loss has occurred. The age estimate is $\simeq$ 2-5 10^3 yr. The high-velocity redshifted emission comes from a structure which becomes "V-like" at velocities close to that of the ambient gas. These results fit nicely with recent magnetohydrodynamical models where a working surface with a cone–like shape creates elongated naked jets containing bullets in their interior.

Key words: stars: formation – ISM: jets and outflows – ISM: individual objects: NGC 1333/IRAS 2 – ISM: molecules – ISM: abundances – radio lines: ISM

1. Introduction

Recent studies of highly collimated outflows (Bachiller 1996) have revealed that there is a class of bipolar outflows which are driven by jets which accelerate the ambient gas through the propagation of large bow shocks (e.g. Raga & Cabrit 1993). The shocked molecular material is well observed in lines of H_2 (e.g. Hodapp & Ladd 1995), SiO (Martín-Pintado et al. 1992), and NH_3 (Bachiller et al. 1993). The shocked gas is highly excited, and has an unusual chemical composition. The latter characteristic is ascribed to shock-processing of the dust grains which enhances the abundances of silicon or sulfur–bearing species. Methanol, CH_3OH, is a molecule which has long been thought to be abundant in grain ice mantles (e.g. Millar et al. 1991; Charnley et al. 1992). It is thus plausible that its abundance might be enhanced in shocks in a manner similar to the molecules discussed above. In a previous paper we presented the first results of a small survey for CH_3OH emission in highly collimated bipolar outflows (Bachiller et al. 1995a). The CH_3OH abundance was observed to be spectacularly enhanced in some outflows, confirming the importance of CH_3OH formation processes from grain desorption. The highly-collimated outflow from Class 0 source NGC 1333/IRAS 2 (hereafter referred to as IRAS 2) is also known to present a high methanol enhancement (Sandell et al. 1994).

The NGC 1333 cluster is placed in the local complex of molecular clouds in Perseus. (Bachiller & Cernicharo 1986). Different estimates of the distance to the complex are in the range 220−350 pc, and we will assume here a value of 300 pc (this choice does not affect any of the conclusions in the paper). The region harbours a dense concentration of young stellar objects (Aspin et al. 1994; Lada et al. 1996) and a correspondingly high number of bipolar outflows. The IRAS 2 outflow stands out as being particularly bright in the emission of some molecules such as CO, CS, and SiO (Sandell et al. 1994, Langer et al. 1996). The flow is highly inclined to the line of sight which causes the two lobes to appear well separated spatially. The outflow is so energetic that it seems to influence the global structure of the surrounding molecular cloud (Warin et al. 1996, Langer et al. 1996, Blake 1996). In many respects, it appears comparable to outflows around other Class 0 sources such as L1448-mm (Bachiller et al. 1995b) or L1157-mm (Gueth et al. 1996). For these reasons, the IRAS 2 outflow is a useful tracer of the characteristics of very young bipolar outflows. In this paper, we present high-resolution maps of the IRAS 2 outflow in several CH_3OH lines. These maps are used to study the excitation and the kinematics of the shock-processed high-velocity gas.

Send offprint requests to: R. Bachiller

2. Observations

2.1. Single-dish observations

The observations were carried out with the IRAM 30-m radio telescope at Pico Veleta (near Granada, Spain) in January 1995. We used three SIS receivers operating in the bands around $\lambda\lambda$ 3, 2, and 1 mm to simultaneously observe some of the J_k=2_k→1_k (96.7 GHz), 3_k→2_k (145.1 GHz), and 5_k→4_k (241.8 GHz) lines of CH_3OH. The system temperature was about 215 K, 190 K and 385 K at 96.7 GHz, 145.1 GHz and 241.8 GHz, respectively. The antenna half-power beamwidths (HPBW) and main beam efficiencies were 25″ and 0.63 at 96.7 GHz, 17″ and 0.56 at 145.1 GHz, and 11″ and 0.42 at 241.8 GHz. Pointing was checked every hour by observing nearby planets or continuum sources, and was found to be accurate to within 3″. The spectrometers were autocorrelators providing a spectral resolution of 0.12 km s^{-1} at 96.7 GHz, 0.16 km s^{-1} at 145.1 GHz, and 0.39 km s^{-1} at 241.8 GHz. All observations were made in position switching mode, and linear baselines were subtracted from the spectra. The calibration of the data was achieved by the chopper wheel method. Intensities are given in units of main beam brightness temperature (T_b).

2.2. Interferometric observations

The interferometric observations of the J_k=2_k→1_k (96.7 GHz) lines were carried out in August and September 1995 with the IRAM 4-antenna array at Plateau de Bure (near Gap, France). Three configurations of array were used (C1, C2, D2) with baselines extending up to 176 m. The antennae were equipped with cooled SIS receivers with typical SSB system temperatures of about 150 K at the observing frequency. The correlator was configured to give a resolution of 202.8 kHz (0.63 km s^{-1} at 96.7 GHz). Phase and amplitude calibration was achieved by observations of 3C84. Typical r.m.s. phase noise was better than 21°. The flux density scale was derived from the observations of 3C454.3 (9-10 August and 1-2 September: 6.4 Jy; 26-27 September: 6.6 Jy). Variations in receiver gain and atmospheric opacity were corrected by frequent measurements of a chopper wheel at ambient temperature. The data were calibrated and analysed with the GILDAS software package developed at IRAM and Observatoire de Grenoble. A mosaic of 3 fields was observed in order to cover the CH_3OH structure observed with the IRAM 30-m antenna. The centers of the fields are at (+70″, –15″), (–55″, +15″) and (–90″, +25″) from the the position of the (sub)millimetre continuum counterpart of IRAS 2 (Sandell et al. 1994; J2000 coordinates: $03^h\ 28^m\ 55.4^s$, +31° 14′ 35.″4). Interferometric images were produced using natural weighting and cleaned in the usual way. The clean beam is 4.″1×3″ at PA 216°. A comparison of the interferometric data with the single-dish data obtained at the 30-m telescope shows that the line intensities from both data sets agree within the usual calibration uncertainties (≃ 20%).

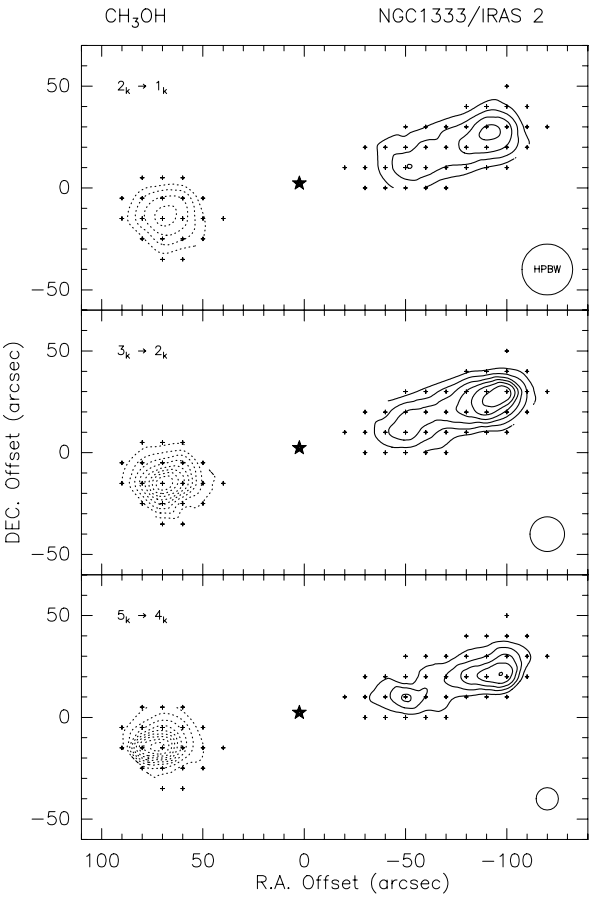

Fig. 1. Contour maps, based upon our 30-m observations, of the integrated (over the whole emission range) 2_k–1_k (upper panel), 3_k–2_k (central panel) and 5_k–4_k (lower panel) CH_3OH emission. The small crosses mark the observed positions, while the black star points out the coordinates of the central source IRAS 2 as measured by Blake (1996). The central (0,0) position is (J2000): $03^h\ 28^m\ 55.4^s$, +31° 14′ 35.″4. The solid line stands for emission blueshifted respect to the velocity of the ambient cloud, while dotted contour is for the redshifted emission (see text). First contour and step are: 10 and 5 K km s^{-1} (red), and 7 and 3 K km s^{-1} (blue) for 2_k–1_k, 10 and 10 K km s^{-1} (red) and 7 and 6 K km s^{-1} (blue) for 3_k–2_k and 5_k–4_k.

3. Single-dish results

Only weak methanol emission has been detected towards the position of IRAS 2, while the regions associated with the two lobes of the outflow are revealed as strong CH_3OH sources, and hence carefully mapped with a 10″ spacing. Fig. 1 shows the maps of the integrated CH_3OH flux for the three groups of transitions. The central position of the map is that of the (sub)millimetre continuum source as measured by Sandell et al (1994). This differs from more recent interferometric observations at 2.7 mm by Blake (1996) which show that the actual position of the source is about 3″ north-east (see his Fig. 2). Fig. 2 displays, as an example, the spectra concerning the central position and the two emission maxima of the two lobes (note that we did not detect the 2_1-1_1 E transition which on the velocity scale of Fig.2 is at ≃ –44 km s^{-1}). The LSR velocity

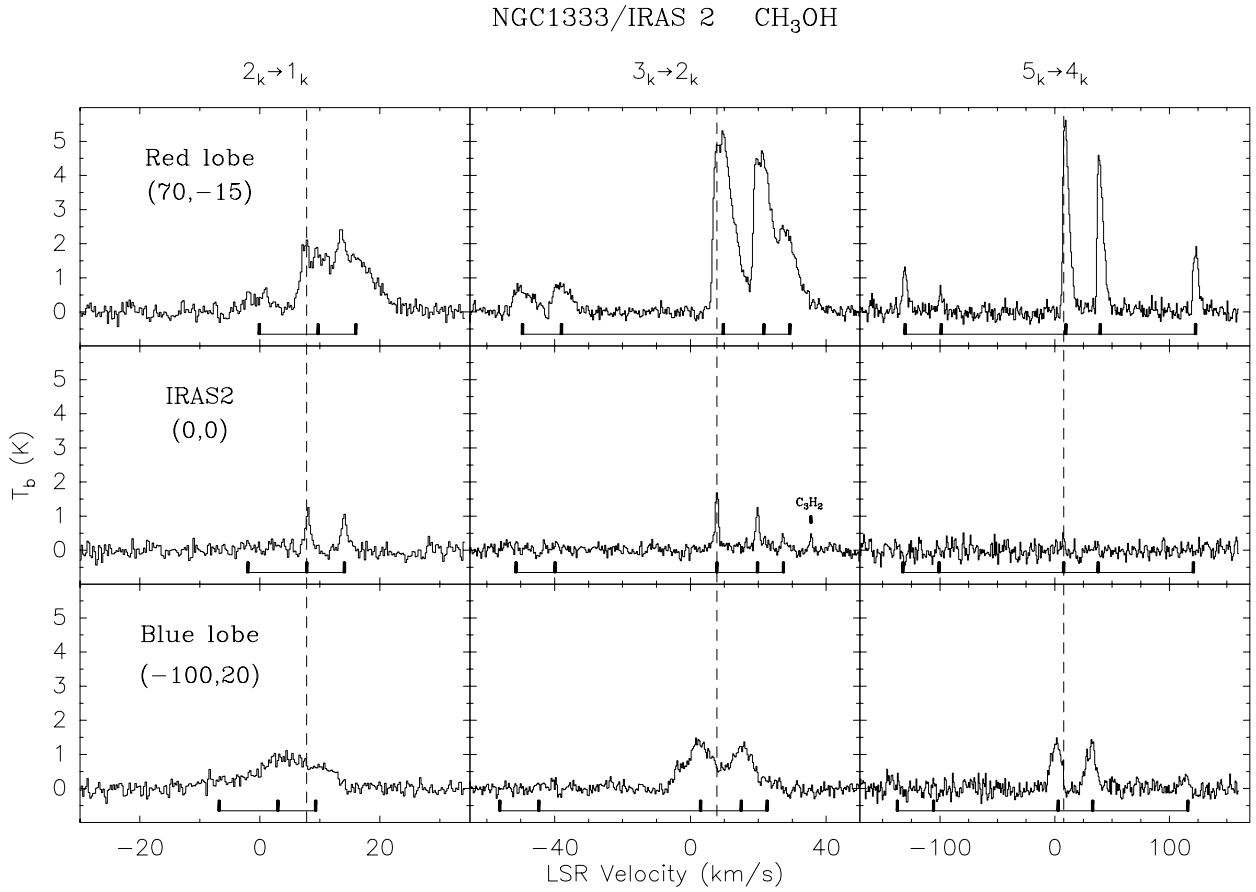

Fig. 2. Spectra obtained towards three representative positions of the IRAS 2 outflow. The (0,0) position is that of the exciting source IRAS 2 (see text), whereas the (70″,–15″) and (–100″,20″) positions correspond to the maxima of the redshifted and blueshifted lobes, respectively. The horizontal axis is the local standard of rest velocity, while the vertical scale is the brightness temperature. The velocity scale of the spectra is calculated with respect to the frequency of the 2_0-1_0 A^+ (96.74142 GHz), 3_0-2_0 A^+ (145.10323 GHz) and 5_0-4_0 A^+ (241.79143 GHz) lines. For each spectrum the predicted position of the CH_3OH lines is shown. The dashed line at 7.8 km s^{-1} indicates the velocity of the quiescent emission, while the velocities at the red and blue lobes are calculated to be 9.6 and 2.9 km s^{-1}, respectively. The 3_{12}–2_{21} line of C_3H_2 is detected towards the (0,0) position: $T_{\rm b}$ = 0.4 (0.1) K, FWHM = 0.7 (0.2) km s^{-1}, $\int T_{\rm b} dv$ = 0.4 (0.1) K km s^{-1}.

of the dense material associated with IRAS 2 is 7.8 km s^{-1}, as determined from the frequency of the 3_0-2_0 A^+ line (145.10323 GHz) and we will assume that this is the systemic velocity of the ambient cloud. The value obtained is in agreement with previous measurements: e.g. 7.6 km s^{-1} from $H^{13}CO^+$ emission (Ward-Thompson et al. 1996) or 7.3 km s^{-1} from the $C^{18}O$ line (Sandell et al. 1994). Table 1 displays, for the spectra reported in Fig. 2, the observed CH_3OH parameters.

Figs. 1 and 2 clearly show that methanol emission observed towards the outflow lobes is significantly shifted from the ambient velocity. Redshifted emission is seen to the south–east of the source whereas blueshifted emission is observed toward the north–west. Moreover, the individual lines are broader and brighter in the lobes of the outflows than towards the central position. The CH_3OH profiles are similar to those of other lines tracing the shocked molecular material (e.g.: CS and SiO, Sandell et al. 1994, Langer et al. 1996). They tend to rise abruptly at the ambient gas velocity and fall off more gradually at high velocities. The methanol emission is spectacularly enhanced in the bipolar outflow, and very clearly is a tracer for the high-velocity gas. For example, the CH_3OH emission due to the 3_0-2_0 A^+ transition coming from the red lobe has a peak $T_{\rm b}$ of about 5.3 K and a FWHM linewidth of about 6.0 km s^{-1}, while the emission towards IRAS 2 has $T_{\rm b} \simeq$ 1.7 K and FWHM $\simeq$ 1.0 km s^{-1}.

In order to estimate the rotational temperatures and column densities, the standard rotation diagram method (e.g. Cummins et al. 1986) has been used. Fig. 3 shows the rotation diagrams for the emission coming from the central object and from the two lobes of the outflow. The least-square fits to all detected lines give rotational temperatures of $T_{\rm rot} \simeq$ 10 K for the ambient gas and $T_{\rm rot} \simeq$ 12-14 K for the outflow (Fig. 3). The total column density averaged over the beam is $N(CH_3OH)$ = 1.2±0.8 10^{14} cm^{-2} for the ambient gas, whereas we find $N(CH_3OH)$ = 1.4±0.2 10^{15} cm^{-2} and 0.8±0.2 10^{15} cm^{-2} for the redshifted and blueshifted lobes, respectively. It is worth noting that the rotation temperature presents only a moderate increase towards the outflow lobes.

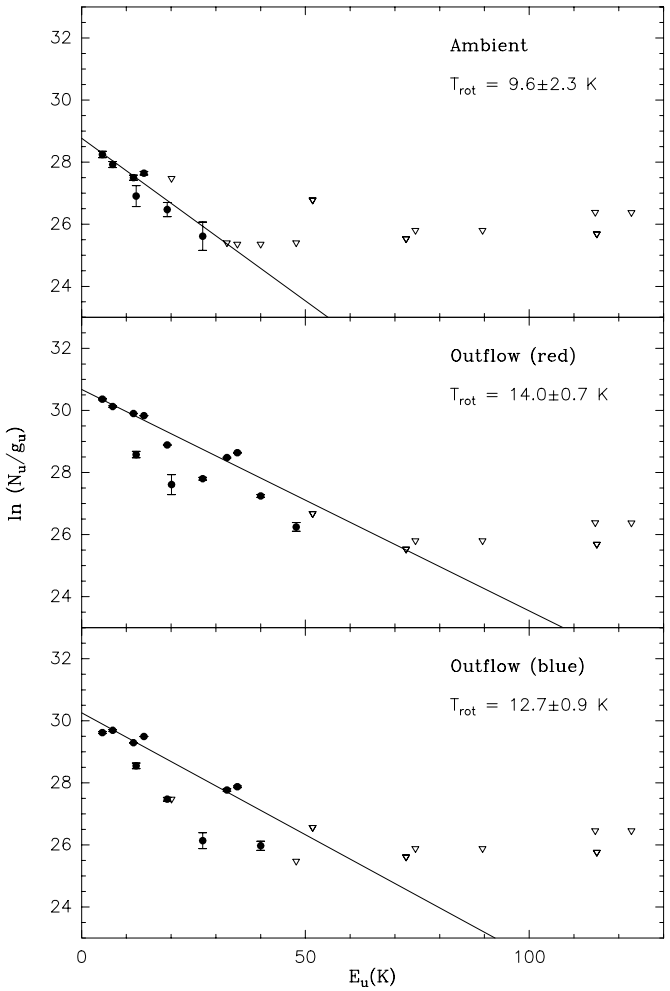

Fig. 3. Rotation diagrams for the methanol transitions measured towards the central objects IRAS 2 and towards the redshifted and the blueshifted lobes of the outflows. The parameters N_u, g_u and E_u are, respectively, the column density, the degeneracy and the energy for the upper levels of the transitions reported. The filled points stand for detections, while the empty triangles are for upper limits. Errorbars are given at one r.m.s. level. The derived values of the rotational temperature are reported.

Table 1. Observed CH_3OH line parameters (see Fig. 2): the main beam brightness temperature (T_b), the LSR velocity (v_{LSR}), the FWHM linewidth and the CH_3OH flux integrated over the whole emission interval of the listed components ($\int T_b dv$). The velocities and the linewidths are calculated using the 2_0-1_0 A^+, 3_0-2_0 A^+ and 5_0-4_0 A^+ lines, respectively

			(+70″,–15″)	(0″,0″)	(–100″,+20″)
2_k-1_k		v_{LSR} (km s^{-1})	+9.6 (0.2)	+7.9 (0.1)	+3.3 (0.2)
		FWHM (km s^{-1})	6.5 (0.2)	1.1 (0.1)	7.2 (0.2)
		$\int T_b dv$ (K km s^{-1})	26.8 (0.8)	2.2 (0.6)	12.6 (0.8)
	T_b (K)	2_1-1_1 E	< 0.5	< 0.4	< 0.4
		2_0-1_0 E	0.5 (0.3)	< 0.4	0.2 (0.1)
		2_0-1_0 A^+	1.5 (0.3)	1.1 (0.2)	0.9 (0.1)
		$2_{-1}-1_{-1}$ E	1.5 (0.3)	0.9 (0.2)	0.6 (0.1)
3_k-2_k		v_{LSR} (km s^{-1})	+9.6 (0.2)	+7.8 (0.1)	+2.9 (0.3)
		FWHM (km s^{-1})	5.8 (0.1)	1.2 (0.1)	7.1 (0.3)
		$\int T_b dv$ (K km s^{-1})	87.0 (0.9)	8.1 (0.8)	23.5 (0.8)
	T_b (K)	$3_{-2}-2_{-2}$ E 3_2-2_2 E	0.7 (0.4)	< 0.4	< 0.4
		3_2-2_2 A^-	0.8 (0.4)	< 0.4	< 0.4
		3_0-2_0 A^+	5.3 (0.4)	1.7 (0.1)	1.4 (0.1)
		$3_{-1}-2_{-1}$ E	4.5 (0.4)	1.2 (0.1)	1.2 (0.1)
		3_0-2_0 E	2.2 (0.4)	0.4 (0.1)	0.2 (0.1)
5_k-4_k		v_{LSR} (km s^{-1})	+9.8 (0.1)	+7.6 (0.3)	+1.3 (0.2)
		FWHM (km s^{-1})	5.9 (0.1)	1.9 (0.8)	9.5 (0.5)
		$\int T_b dv$ (K km s^{-1})	90.9 (1.2)	1.2 (0.8)	28.4 (1.3)
	T_b (K)	5_2-4_2 E $5_{-2}-4_{-2}$ E	1.2 (0.4)	< 0.5	< 0.5
		5_1-4_1 E	0.6 (0.4)	< 0.5	< 0.5
		5_0-4_0 A^+	5.6 (0.4)	0.5 (0.1)	1.4 (0.2)
		$5_{-1}-4_{-1}$ E	4.5 (0.4)	< 0.5	1.2 (0.2)
		5_0-4_0 E	1.9 (0.4)	< 0.5	0.4 (0.1)

However, as discussed by Bachiller et al. (1995a), in the range of physical conditions connected with molecular outflows, the methanol molecule, due to the peculiarities of the its energy level structure, is very subthermally excited. A detailed study of the methanol excitation and a discussion on the measuring of T_{rot} are presented in Sect. 5.

With the aim of obtaining an estimate of the CH_3OH abundances, the H_2 column densities towards the central object and the outflow have been derived by comparing with the CO and $C^{18}O$ data previously reported by Sandell et al. (1994). For the ambient gas the $C^{18}O$ observations have been used, assuming an excitation temperature T_{ex} equal to 15 K and a $C^{18}O$ abundance $[C^{18}O]/[H_2] = 2\ 10^{-7}$. The H_2 column density in the direction of the lobes of outflow has been derived with the CO data and with the assumption of $[CO]/[H_2] = 10^{-4}$ and T_{ex} = 100 K. The assumption of a high value for the excitation temperature for the IRAS 2 outflow is justified by the detection of relatively bright NH_3(3,3) emission towards the two lobes (100-m Effelsberg unpublished data), indicating gas kinetic temperatures in excess of 60 K, similar to the other outflows investigated by Bachiller et al. (1993, 1995a, 1995b). For so high temperatures the CO broad wings are expected to be optically thin. The derived values, N_{H_2} = 2.0 10^{22} cm^{-2} (ambient gas) and N_{H_2} = 5.8 10^{20} cm^{-2} (high-velocity gas), yield CH_3OH abundances $[CH_3OH] = 6.0\ 10^{-9}$ for the ambient gas and $[CH_3OH] = 1.9\ 10^{-6}$ for the high-velocity gas. Thus, we find that the methanol abundance is enhanced by a factor $\simeq$ 300 toward the shocked molecular gas of the outflow. This result is in agreement with that obtained for the young bipolar outflows L1157, NGC2071 and IRAS03282 (Bachiller et al. 1995a).

In order to investigate the outflow kinematics, we present in Fig. 4 the velocity channel maps of the CH_3OH 5_0–4_0A^+ emission, i.e. of the strongest component of the 1mm group of transitions, investigated with an angular resolution of 11″. There is an indication that the shape of the redshifted CH_3OH source (placed at the SE from IRAS 2) depends on the LSR velocity: emission at high velocity is associated with an elongated structure, located along the main axis of the bipolar outflow whereas the lower velocity gas has more circular contours. Moreover, the blueshifted structure (placed at the NW

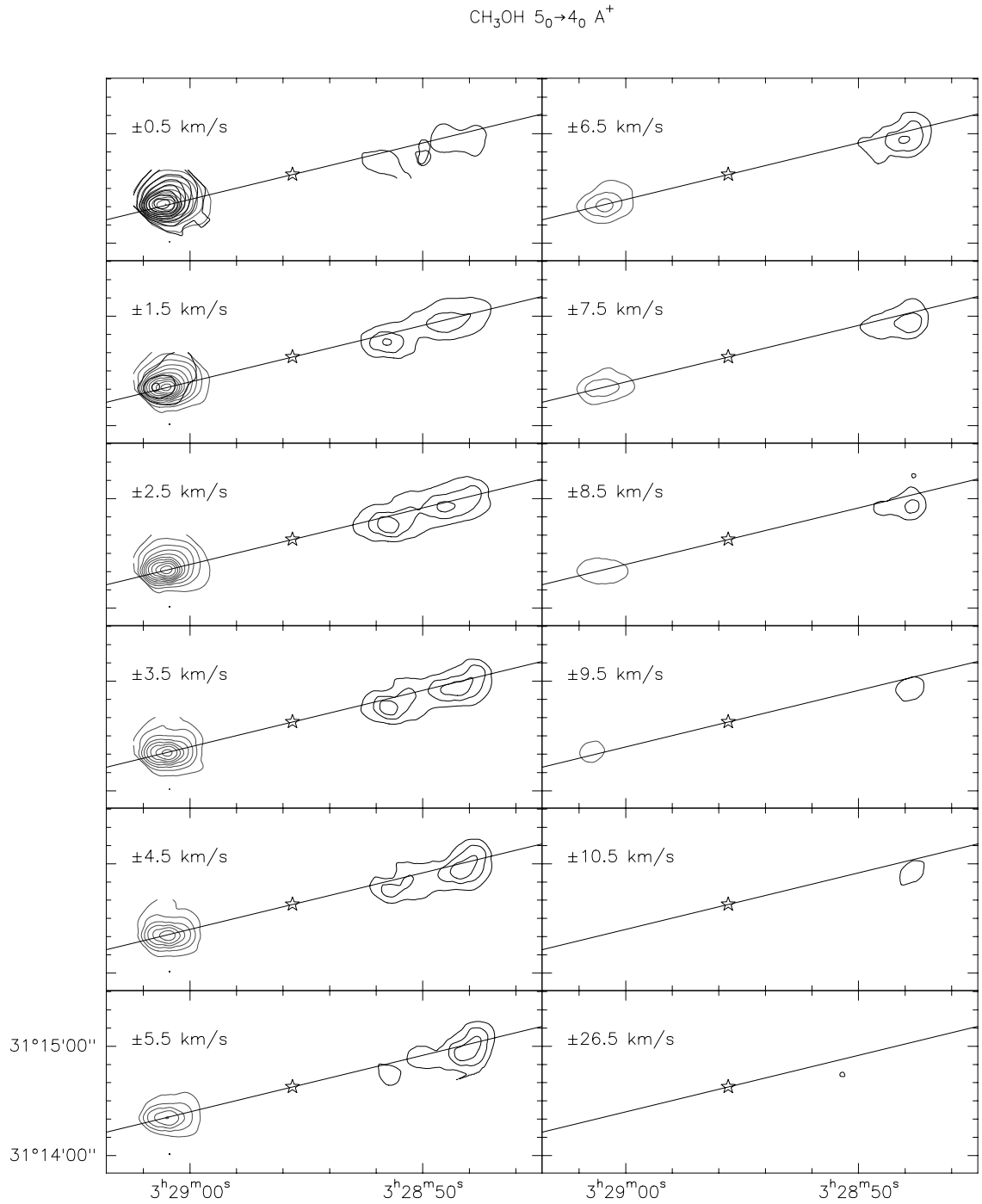

Fig. 4. Channel maps of the CH_3OH 5_0–4_0A^+ emission detected with the 30-m antenna, integrated over velocity intervals of 1 km s^{-1} wide. The white star stands for the coordinates of the central source IRAS 2 as measured by Blake (1996), while the straight line points out the direction of the outflow. The contours placed at the south-east of IRAS 2 are due to redshifted emission, whereas the contours at the north-west are blueshifted emission. Nevertheless, some overlap of redshifted and blueshifted emission is observed at low velocities in the south-east lobe (the left region in the panels at $\pm$0.5 and $\pm$1.5 km s^{-1}). The contour levels range from 0.50 to 6.00 Jy km s^{-1} by step of 0.50 Jy km s^{-1}. The central LSR velocities for each interval, obtained with respect to the LSR velocity of the ambient gas, are indicated in the upper left corner of each panel.

from IRAS 2) suggests the presence of different clumps along the outflow axis. A surprising feature is that we tentatively detect a small clump of CH_3OH emission at very high velocity, –26.5 km s^{-1}, respect to the LSR velocity of the ambient gas (the single contour on the bottom-right panel of Fig. 4). The FWHM of this feature is about 5 km s^{-1} and its location is at (-60″,+10″) from the position of the (sub)millimetre continuum counterpart of IRAS 2. The CH_3OH 2_k–1_k and 3_k–2_k emission

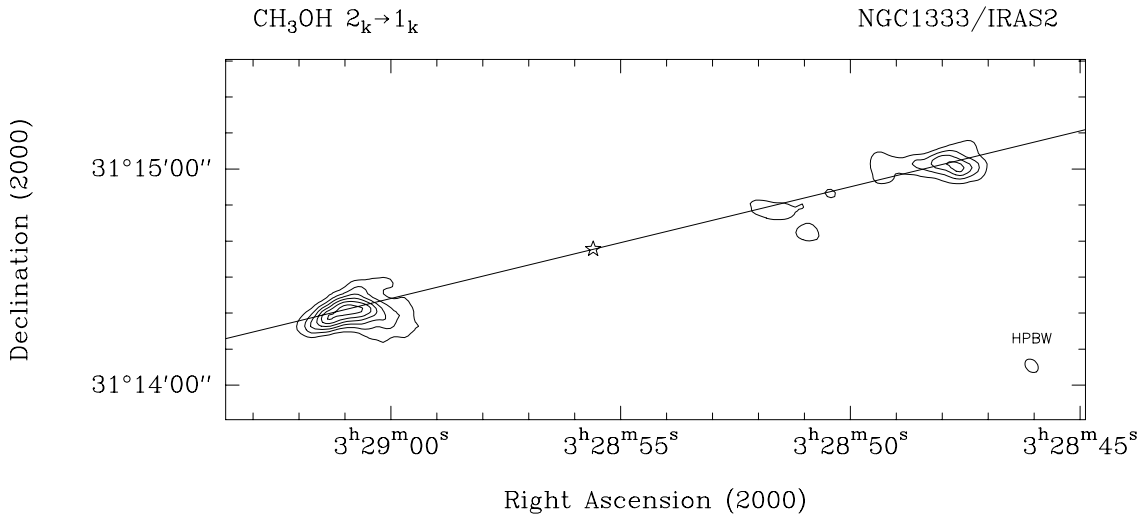

Fig. 5. Interferometric map of the CH_3OH 2_k–1_k emission towards IRAS 2. The contour levels range from 4 to 36 Jy km s^{-1}/beam by step of 6 Jy km s^{-1}/beam (63 K km s^{-1}). Symbols are drawn as in Fig. 4. The contours placed at the south-east of IRAS 2 are mainly due to redshifted emission, whereas contours at the north-west are blueshifted emission (see velocity channel maps in Fig. 6).

reveals a similar kinematic structure, but less clearly because of (i) the lower angular resolution respect to the 1mm lines and (ii) the blend of the different methanol lines (see Fig. 2). In any case, Fig. 4 shows that the methanol emitting structures are extremely compact and that one needs higher angular resolution to study properly the outflow kinematics.

4. Interferometric results

Fig. 5 shows the map of the CH_3OH 2_k–1_k emission associated with the lobes of the IRAS 2 outflow. The 3mm lines of CH_3OH have three main components, as seen in Fig. 2. To investigate the kinematics of the high velocity gas it is necessary to deblend such components. In order to obtain the intensity of the strongest 2_0–1_0A^+ line, we have fitted a system of three gaussians with fixed linewidths and velocities separated by the amounts expected on the basis of laboratory frequencies. The interferometric map confirms the close association of CH_3OH with the lobes of the bipolar CO outflow (Sandell et al. 1994) and, in particular, with its endpoints. Moreover, Fig. 5 shows that the methanol emission is confined in two elongated jet-like structures located along the main axis of the outflow. A rough estimate of the collimation factor based upon the ratio between the jet length (about 200″) and its width leads to a factor of $\simeq$ 20, making the present outflow one of the best collimated flows ever detected. It is worth noting that the shape of the red shifted lobe does not resemble that expected for a bow-shock but is more elongated toward the direction of IRAS 2. On the other hand, the blueshifted methanol consists of a chain of several knots. We will refer to such compact structures as "bullets".

More information about the kinematical structure of the IRAS 2 outflow can be obtained from the channel maps, displayed in Fig. 6. These show that the methanol 2_0–1_0A^+ emission extends in velocity up to about $\pm$ 10 km s^{-1} with respect to the LSR velocity of the ambient gas associated with IRAS 2. Moreover, the occurrence of a CH_3OH clump associated with a velocity of –26.5 km s^{-1}, suggested by the single-dish channel maps (see Fig. 4), is confirmed by the interferometric observations (single contour in bottom-right panel of Fig. 6). The clump is hardly resolved by the $\sim 3''$ beam and its estimated size is about $4''$. Fig. 6 confirms also that the blueshifted lobe consists of different bullets travelling at different velocities.

The methanol emission at the highest velocities is aligned on a well defined jet axis with a width of about $5''$, corresponding to $\simeq$ 1500 AU at a distance of 300 pc. However, it is possible to see that the structure of the CH_3OH emission varies significantly with velocity. In particular, the high-velocity redshifted emission comes from a jet-like structure that assumes a peculiar "V-like" shape as the velocity approaches that of the ambient gas. The "V-like" shape, which is particularly well observed in the first panel of Fig. 6 (see zoom of such panel in Fig. 7), is similar to the head of an imaginary arrow which would point away to the south-east from IRAS 2.

Fig. 6 indicates also that if we take into account just the low-velocity CH_3OH emission, the red- and the blueshifted emissions have similar spatial distributions, overlapping quite well. This effect (present also in the channel maps drawn using the single-dish data, in Fig. 4) is particularly clear for the red lobe of the outflow, as seen in Fig. 7. Such a configuration suggests that the V-like shape outlines a structure which could be partly empty, or filled with low density material. This could correspond to the two sides of a shock expanding into the ambient clump. It is also probable that the axis of the outflow is located in a plane close to that of the sky. Actually, the low-velocity blueshifted emission of the red lobe is probably due to the part of the V-like structure directed towards us, because of its expansion motion and of the high inclination of the outflow axis. This geometric picture is supported by the low velocity extent of the IRAS 2 flow relative to the ambient medium (the bulk

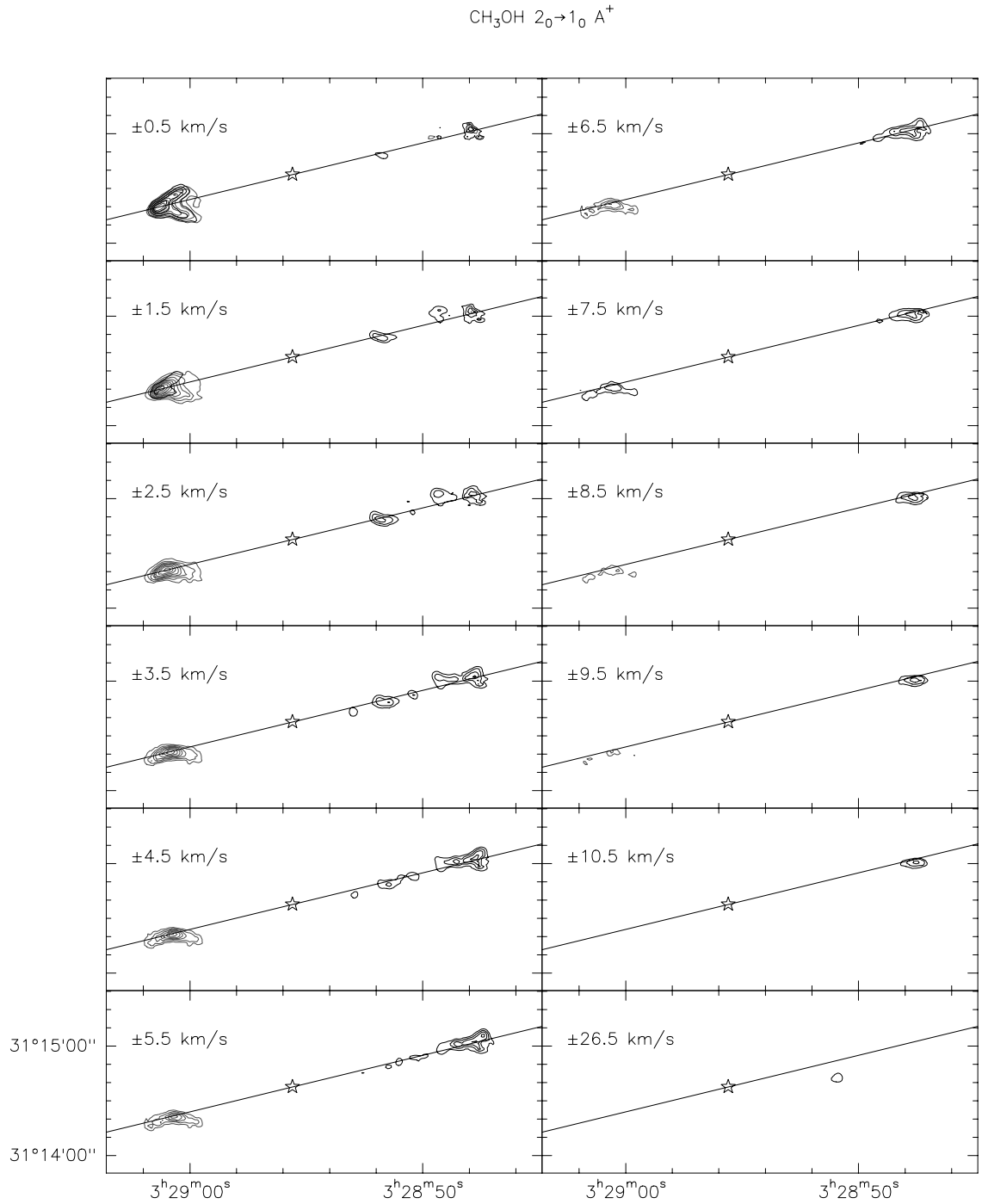

Fig. 6. Channel maps of the CH_3OH 2_0–1_0A^+ emission detected with the IRAM interferometer, integrated over velocity intervals of 1 km s^{-1} wide. Symbols are as in Fig. 4. The central LSR velocities for each interval, measured with respect to the LSR velocity of the ambient gas, are indicated in the upper left corner of each panel. Also similar to Fig. 4, the contours placed at the south-east of IRAS 2 are due to redshifted emission, whereas the contours at the north-west are blueshifted emission. Nevertheless, some overlap of redshifted and blueshifted emission is observed at low velocities in the south-east lobe (the left region in the panels at $\pm$0.5 and $\pm$1.5 km s^{-1}). To visualize such an overlap, a zoom of the south-east region of the $\pm$0.5 km s^{-1} panel is shown in Fig. 7. The contour levels range from 0.15 to 1.50 Jy km s^{-1}/beam by step of 0.15 Jy km s^{-1}/beam (1.58 K km s^{-1}).

of the emission is within $\pm$ 10 km s^{-1}) and, above all, by the large spatial separation between the two CH_3OH lobes of the outflow.

5. Methanol excitation

We have modeled the methanol excitation using a 100 level LVG code which considers levels up to J = 15 and K up to 3 in both A and E-type methanol. The code has been used and

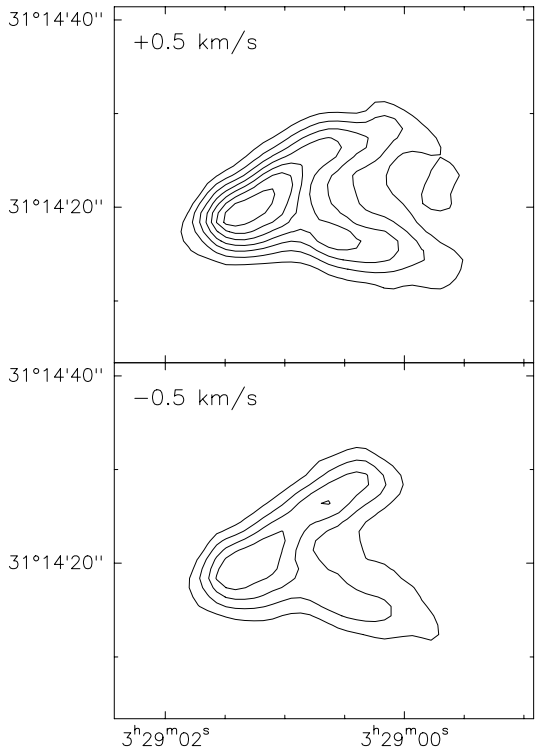

Fig. 7. Methanol low-velocity (± 0.5 km s^{-1} with respect to the central velocity of the ambient gas) 2_0–1_0A$^+$ emission towards the south-east lobe of IRAS 2, detected with the IRAM interferometer and integrated over velocity intervals of 1 km s^{-1} wide. This is a zoom of the bottom left region in the first panel of Fig. 6 to visualize the overlap of blueshifted and redshifted emission. Contour levels are as in Fig. 6. Note the peculiar "V-like" shape which resembles the head of an imaginary arrow pointing away to the south-east from IRAS 2 (see text for details).

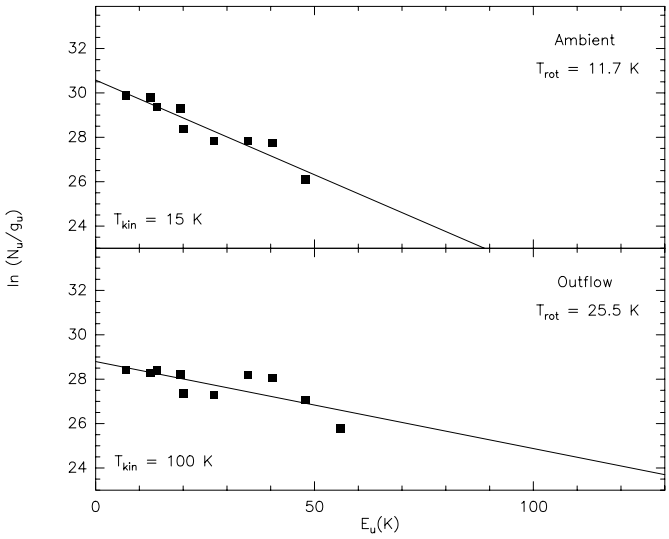

Fig. 8. Example of synthetic CH_3OH rotation diagrams, calculated assuming $N(CH_3OH)/FWHM = 10^{14}$ cm^{-2} (km s^{-1})$^{-1}$, $n_{H_2} = 10^6$ cm^{-3} and: (upper panel) $T_{\rm kin}$ = 15 K; (bottom panel) $T_{\rm kin}$ = 100 K.

briefly described by Menten et al. (1988) and by Johnston et al. (1992). The collisional rates used are based upon laboratory work by Lees & Hacque (1974) and are somewhat uncertain. As a consequence, the density estimates which we derive need confirmation. Nevertheless, we note that methanol has great potential as a density estimator due to its property of having groups of lines of widely differing radiative lifetimes and excitations (such as the $J+1$, $K-J$, K series examined here) at similar frequencies.

We have thus run two grids of models varying density and methanol column density with the aim of simulating the observations of the ambient gas and the shocked gas respectively. Based upon our ammonia results, we assume a temperature of 15 K for the ambient gas and 100 K for the shocked outflow emission observed in the lobes (see Sect. 3). Then using the computed line intensities, we have constructed synthetic rotation diagrams, similar to those resulting from the observations (see Fig. 3). In this way, we estimated model rotation temperatures. An example of such a synthetic diagram is presented in Fig. 8, together with a fit to a Boltzmann population distribution. In order to simulate the observational approach, we have in this simulation neglected all transitions with intensity less than 0.1 K. Fig. 8 illustrates the point that fitting a non-LTE population distribution with a single rotation temperature cannot be expected to yield unique results. The theoretical intensities clearly do not allow a fit to a straight line in a plot of ln(level column density) against excitation. A consequence is that the rotation temperature which one derives depends (occasionally sensitively) on the choice of observed lines. Thus dispersion of observed line intensities relative to a Boltzmann fit is to be expected and indeed potentially can yield useful information on departures from LTE. It is consequently often more useful to compare various observed and predicted line ratios in order to derive physical quantities such as density and temperature from the observed intensities.

The methanol rotation temperature derived in the manner outlined above gives nevertheless a rough measure of the level of methanol excitation. For optically thin conditions, $T_{\rm rot}$ in general increases from low values at densities of order 10^4 cm^{-3} to values close to the assumed kinetic temperature ($T_{\rm kin}$) at densities of order 10^8 cm^{-3}. Fig. 9a shows some sample results where we have confined ourselves to cases where the transitions of interest are at most moderately optically thick as seems to be the case towards IRAS 2. One sees from Fig. 9a that values of $T_{\rm rot}$ below 25 K as observed are expected for densities below 3.0 10^6 cm^{-3}. This is almost irrespective of assumed temperature. Below this limit, $T_{\rm rot}$ is rather insensitive to density and temperature. For example, for $T_{\rm kin}$ = 100 K and $N(CH_3OH)/FWHM$ = 1.0 10^{14} cm^{-2} (km s^{-1})$^{-1}$, $T_{\rm rot}$ only increases from 12 to 25 K while the density increases from 1.0 10^4 to 3.0 10^6 cm^{-3}. A similar situation happens for cold gas: for $T_{\rm kin}$ = 15 K and $N(CH_3OH)/FWHM$ = 1.0 10^{14} cm^{-2}, when the density increases from 1.0 10^4 to 3.0 10^6 cm^{-3}, $T_{\rm rot}$ only goes from 8 to 12 K. We thus conclude that, for the range of methanol excitation discussed here, the parameter $T_{\rm rot}$ only allows limits to be placed upon the physical conditions in the gas.

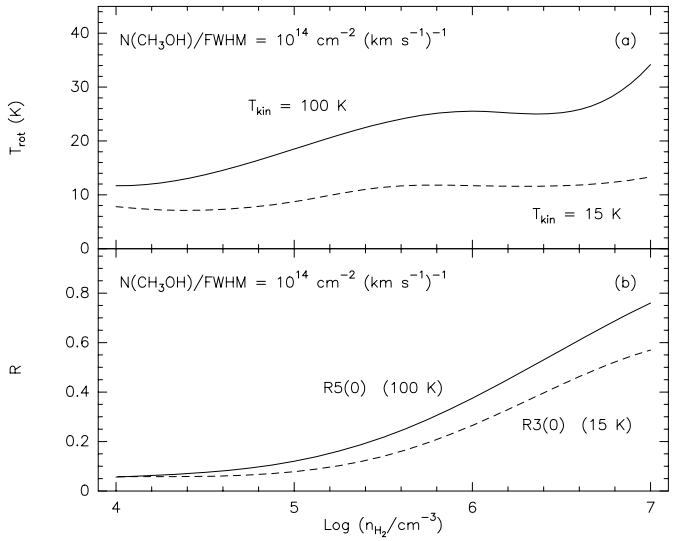

Fig. 9. a The rotation temperature as a function of the $n_{\rm H_2}$ density assuming N(CH$_3$OH)/FWHM = 1.0 10^{14} cm^{-2} (km s^{-1})$^{-1}$ and $T_{\rm kin}$ = 15 K (dashed line) or $T_{\rm kin}$ = 100 K (continuous line); **b** The parameters $R3(0)$ (calculated assuming $T_{\rm kin}$ = 15 K, dashed line) and $R5(0)$ ($T_{\rm kin}$ = 100 K, continuous line) as a function of the $n_{\rm H_2}$ density. N(CH$_3$OH)/FWHM is assumed 1.0 10^{14} cm^{-2} (km s^{-1})$^{-1}$.

On the other hand, some methanol line ratios can in principle provide sensitive measurements of the excitation. After considering several possibilities, we found that the ratio $R3(0)$ defined as $T_{\rm b}(3_0 - 2_0E)/T_{\rm b}(3_{-1} - 2_{-1}E)$ can be used to give a good estimate of the density for low kinetic temperatures. For instance, for $T_{\rm kin}$ = 15 K and N(CH$_3$OH)/FWHM = 1.0 10^{14} cm^{-2}, when the density increases from 1.0 10^4 to 3.0 10^6 cm^{-3}, $R3(0)$ increases from 0.06 to 0.4. For higher temperatures, one can measure the $5_{\rm k}$–$4_{\rm k}$ lines and use the ratio $R5(0)$: for $T_{\rm kin}$ = 100 K and N(CH$_3$OH)/FWHM = 10^{14} cm^{-2}, and for densities increasing from 1.0 10^4 to 3.0 10^6 cm^{-3} $R5(0)$ varies from 0.06 to 0.6. Using these ratios, we have estimated the gas density in the cold gas around the position of IRAS 2, and in the warm shocked regions. The measured value of $R3(0)$ is 0.33 for the quiescent gas, whereas R5(0) is in the range 0.33 to 0.42 in the outflow. Thus, by assuming that the gas kinetic temperature is 15 K and 100 K in both regions, respectively, we find (see Fig. 9b) that the density is close to 10^6 cm^{-3} both in the quiescent gas around the star, and in the shocked regions.

It is also interesting to study the ratio $R5(0)$ as a function of the velocity. In fact, we found that there is a systematic variation of the $R5(0)$ ratio along the observed line profiles, with the highest values found at the highest velocities. This seems to indicate that the methanol excitation is the highest for the gas at the extreme velocities. However, the methanol abundance could also be varying with the velocity. We are presently starting further high resolution observations which will allow a more detailed study of the dependence of the chemistry and excitation with the velocity.

6. Discussion

The data reported in this paper shows that the IRAS 2 source gives rise to one of the most spectacular molecular outflows driven by Class 0 objects. In particular, its high degree of collimation, its jet-like structure and its high geometric inclination cause this object to be one of the best laboratories for the investigation of the process of mass loss associated with the earliest evolutionary stages of low-mass star forming regions and for the comparison of the observations with theoretical models.

Previous results (Sandell et al. 1994) have suggested that IRAS 2 is a protostellar binary, where each star drives a bipolar molecular outflow. The youngest source, detected as (sub)millimetre source (and pointed out in the figures of the present paper), is the driving source of an outflow roughly directed along the E-W direction; there is also however a N-S outflow present, driven, according to the authors, by a more evolved source located about ten arcseconds west of IRAS 2. While the present data do not allow any conclusions to be drawn about the N-S outflow, they suggest that the E-W one is very energetic and still interacting with the ambient medium. Our results seem to be in good agreement with the observations of IRAS 2 and of the redshifted lobe reported by Blake (1996). He found a jet-like structure traced by high-velocity SiO (J=2–1) emission which fits into the redshifted CH$_3$OH lobe reported in Fig. 5. Moreover, his CS (J=2–1) image highlights the importance of the interaction of the molecular outflow with the ambient medium. It is interesting to note that the low-velocity CS structure has a V-like shape similar to what we find for CH$_3$OH, which suggests that its origin comes from the encounter of the jet driven by IRAS 2 with the molecular cloud. The present CH$_3$OH results give a picture of both the lobes of the E-W outflow and underline the importance of the ambient medium in shaping the flow coming from the central stellar object. Fig. 6 clearly shows that the initial jet-like structure assumes a V-like shape which is far from the classical bow-shock, but gives evidence of the deceleration of the high-velocity flow due to the interaction with the surrounding ambient gas. It is worth noting that the V-like structure is not symmetric relative to the outflow axis and that this could reflect the geometry of the ambient clump-jet complex.

Regarding the chemistry, we point out that the present observations confirm the close correlation of methanol emission with the molecular gas shocked by the occurrence of an outflow. The calculated enhancement of methanol towards the molecular outflow with respect to the central object and the interferometric maps clearly show that CH$_3$OH emission comes from the endpoints of the lobes of the outflow, where shock waves compress and heat the ambient gas, triggering a chemistry different from that operating in quiescent gas.

The observations reported have provided a clear evidence that the IRAS 2 outflow is representative of episodic mass loss of its driving protostellar object, since the blueshifted lobe is composed of several bullets at different velocities. This allows us to give a rough estimate of the age of the outflow, by comparing the distance between the farthest bullet and the central object: about 5 10^3 yr (2 10^3 yr) assuming

15° (5°) as the angle between the direction of the outflow and the plane of the sky (see Sect. 4). A rough estimate of the time elapsed between successive ejections of bullets by the central (proto)stellar object can be obtained by comparing the positions and the velocities of different bullets located along the main direction of the outflow. In this way, we obtain a time interval of 2 10^3 yr (6 10^2 yr). It is worth noting that, regarding this chain of bullets, there is an indication that the bullet velocity increases with distance from the central star. There are several possible explanations for this trend. It could be that these condensations (located along the main axis of the blueshifted lobe) are accelerating as they flow outward from the star. A second possibility is that the power of the ejection process that has produced these bullets has decreased. Finally, we cannot rule out that the angle of inclination of the outflow has changed due to precession.

If we consider the CH_3OH emission located at –26.5 km s^{-1}, the age estimate leads to a value of 400 yr (130 yr) indicating that this bullet is the youngest of the structures detected towards the present outflow. Moreover, it is located away from the outflow axis, suggesting that precession of the outflow axis is taking place. Similar precession effects have been also seen in the L1157 outflow (Gueth et al. 1996).

Another interesting point concerns the shape of the end–point of the redshifted CH_3OH lobe, i.e. what we have called a V-like structure. Our observations, the observations of Blake (1996), and the CO data reported by Sandell et al. (1994) all show an elongated structure quite different from that expected for a classical bow-shock. Similar morphologies have been also observed in the SiO emission of other outflows such as L1157, L1448 and HH211 (Gueth et al. 1996, Gueth 1997). We believe that the V-like structure seen by us is due to similar basic mechanisms as those operating in the flows studied by Gueth et al. Clarke et al. (1986) have published simulations of magnetohydrodynamical (MHD) jets and shown that these jets produce a structure they call a nose cone, i.e. having a conical shape, at its head. Moreover, the authors predict that these MHD jets should present spaced emission bullets and should appear quite naked, without an extended cocoon around them. Recently, Ouyed et al. (1997) have reported time-dependent MHD simulations of the onset and collimation of outflows from the surface of a keplerian accretion disk for different initial magnetic configurations. They presented, among their models, the prediction of episodic outflows associated with highly collimated jets with density structures dominated by discrete bullets. The working surface in these simulations has the shape of a cone that advances with a swept-back shock along its sides (see their Fig. 4). Moreover, the formation of a cone-like working surface should deplete the available material capable of forming an extended cocoon, with the consequent occurrence of a naked jet.

Our observations are in general agreement with these theoretical models, since our CH_3OH outflow clearly presents a highly collimated naked structure containing different bullets and, above all, since we found evidence that the interaction of the observed jet with the ambient medium produces a structure similar to a geometrical projection of a cone. In particular, the simulations of episodic outflows reported by Ouyed et al. (1997) foresee an average speed of the material of about 0.5 times the Kepler speed at the innermost disk radius, taken equal to three times the stellar radii. This prediction can be compared with our observations, since an estimate of the FIR luminosity of 30 $L_\odot$ (Sandell et al. 1994), assuming a distance of 300 pc, is available. Substituting the corresponding mass ($\simeq 2.3\ M_\odot$) into the expression of the Kepler speed, we obtained $\simeq$ 200 km s^{-1}. Thus, if the IRAS 2 outflow can be represented by the MHD models of Ouyed et al. (1997), we expect a velocity of about 100 km s^{-1} for the material of the jet. In order to fit this prediction with the observed value and considering an average value of 10 km s^{-1} for the observed radial LSR velocity, we need an angle between the direction of the outflow and the plane of the sky of about 6°. Taking into account all the uncertainties in the assumptions used in this calculation (for instance, we have neglected the possible binary nature of IRAS 2, as suggested by Sandell et al. 1994), this estimate is in agreement with the high inclination of the outflow deduced in Sect. 4. Thus, the present results support the scenario where magnetic fields held in the accretion disk can accelerate and collimate a mass loss process into jets, perhaps with episodic knots within their structure.

7. Conclusions

High resolution maps of the Class 0 NGC 1333/IRAS 2 outflow in several CH_3OH lines at 1, 2 and 3 mm are presented. The main results are the following:

1. Only weak methanol emission has been detected towards the position of the central object IRAS 2, while strong and very broad lines are observed towards the endpoints of the two outflow lobes. The CH_3OH emission is definitely shifted from the ambient medium LSR velocity: redshifted emission comes from the S-E lobe, while blueshifted methanol has been detected towards the N-W lobe. A small inclination of the outflow axis to the plane of the sky has been deduced.
2. The methanol abundance is enhanced by a factor $\simeq$ 300 toward the shocked molecular gas with respect to the value deduced for the position corresponding to the central (proto)stellar object.
3. Theoretical line intensities obtained using radiative model calculations do not allow a fit to a straight line in a plot of ln(level column density) against excitation. As a consequence, fitting the population distribution with a single rotation temperature leads to a value which can be used only to place limits upon the physical parameters of the gas. On the other hand, methanol line ratios allow us to obtain sensitive measurements of the CH_3OH excitation. We infer a density close to 10^6 cm^{-3} for the ambient gas and for the shocked regions.
4. The interferometric map shows that the CH_3OH emission is confined in two elongated jet-like structures located along the main direction of the outflow. The factor of collimation is about 20, one of the largest factors ever derived for molecular outflows. The methanol emission extends in velocity up to about $\pm$ 10 km s^{-1} with respect to the ambient medium;

a molecular clump with a velocity of about –26.5 km s^{-1} has been also detected. The blueshifted lobe consists of different bullets located at different velocities, indicating the occurrence of episodic mass loss.

5. An approximate age of $\simeq$ 2-5 10^3 yr for the outflow has been derived, while the estimated elapsed time between successive ejections of bullets is $\sim 2\ 10^3$ yr. For the bullet at –26.5 km s^{-1}, we found an age of just $\simeq$ 130-400 yr and we conclude that the jet axis may be precessing.
6. There is a clear relationship between the velocity of the redshifted methanol emission and its shape: the high-velocity emission comes from a jet-like structure. At lower velocities close to that of the ambient material, a V-like structure is observed that differs considerably from expectations for a classical bow shock. This result can be understood on the basis of recent MHD theoretical models which, for certain magnetic fields configurations, predict a working surface with a shape of a cone creating elongated naked jet-like structures with several bullets within.

Acknowledgements. This work has been partially supported by the Spanish DGES under grant PB96-0104. C.M.W. acknowledges travel support from ASI grant ARS-96-66 as well as CNR grant 97.00018.CT02

References

Aspin C., Sandell G., Russel A.P.G., 1994, A&AS 106, 165
Bachiller R., 1996, ARA&A 34, 111
Bachiller R., Cernicharo J., 1986, A&A 166, 283
Bachiller R., Martín-Pintado J., Tafalla M., Cernicharo J., Lazareff B., 1990, A&A 231, 174
Bachiller R., Martín-Pintado J., Fuente A., 1993, ApJ 417, L45
Bachiller R., Liechti S., Walmsley C.M., Colomer F., 1995a, A&A 295, L51
Bachiller R., Guilloteau S. Dutrey A., Planesas P., Martín-Pintado J., 1995b, A&A 299, 857
Blake G.A., 1996, in van Dishoeck E.F. (ed) Proc. IAU Symp. 178, Molecules in Astrophysics: Probes and Processes, Kluwer, Dordrecht, p. 31
Charnley S.B., Tielens A.G.G.M., Millar T.J., 1992, ApJ 399, L71
Clarke D.A., Norman M.L., Burns J.O., 1986, ApJ 311, L63
Cummins S.E., Linke R.A., Thaddeus P., 1986, ApJS 60, 819
Gueth F., 1997, Ph.D. thesis, Univ. Grenoble, France
Gueth F., Guilloteau S., Bachiller R., 1996, A&A 307, 891
Hodapp K.-W., Ladd E.F., 1995, ApJ 453, 715
Johnston K.J., Gaume R., Stolovy S., Wilson T.L., Walmsley C.M., Menten K.M., 1992, ApJ 385, 232
Lada C.J., Alves J., Lada E.A., 1996, AJ 111, 1964
Langer W.D., Castets A., Lefloch B., 1996, ApJ 471, L111
Lees R.M., Haque S.S., 1974, Canadian J. Phys. 52, 2250
Martín-Pintado J., Bachiller R., Fuente A., 1992, A&A 254, 315
Menten K.M., Walmsley C.M., Henkel C., Wilson T.L., 1988, A&A 198, 253
Millar T. J., Herbst E., Charnley S.B., 1991, ApJ 369, 147
Ouyed R., Pudritz R.E., Stone J.M., 1997, Nature 385, 409
Raga A., Cabrit S., 1993, A&A 278, 267
Sandell G., Knee L.B.G., Aspin C., Robson I.E., Russell A.P.G., 1994, A&A 285, L1
Ward-Thompson D., Buckley H.D., Greaves J.S., Holland W.S., André P., 1996, MNRAS 281, L53
Warin S., Castets A., Langer W.D., Wilson R.W., Pagani L., 1996, A&A 306, 935